INTERNATIONAL JOURNAL FOR NUMERICAL METHODS IN FLUIDS, VOL. 18, 189–214 (1994)

ON THE DIFFICULTIES AND REMEDIES IN ENFORCING THE *div* = 0 CONDITION IN THE FINITE ELEMENT ANALYSIS OF THERMAL PLUMES WITH STRONGLY TEMPERATURE-DEPENDENT VISCOSITY

D. L. COULLIETTE*

Department of Mathematics, Florida State University, Tallahassee, FL 32306, U.S.A.

AND

M. KOCH

Supercomputer Computations Research Institute, Department of Geology and Geophysical Fluid Dynamics Institute, Florida State University, Tallahassee, FL 32306, U.S.A.

SUMMARY

A finite element (FE) analysis of experimentally observed creeping thermal plumes in a medium whose viscosity is strongly temperature-dependent is performed. Such plumes are considered to play an important role in numerous geological processes and numerical modelling is often the only option to study their physics. Initial simulations by means of the general-purpose Galerkin finite element package NACHOS-II demonstrated serious deficiencies of the method in modelling plumes with large viscosity contrasts, in spite of several options for the solution (mixed or penalty formulation) and the elements (continuous or discontinous pressure). In agreement with observations from FE simulations of isothermal Stokes flow in other studies, we have isolated the violation of the div = 0 or incompressibility constraint as the major culprit in the failure of the FE method. It is demonstrated that the *a posteriori* computed discrete divergence (DDIV) can be used as a diagnostic tool to evaluate the reliability of the FE solution and to rank the solution and element options provided in the NACHOS code. On the basis of these considerations, the combination of the mixed method with a Q_2–P_1 (discontinuous pressure) element turns out to be the most suitable for the present plume problem but is still unable to sufficiently enforce the div = 0 condition. With a goal to remedy this detrimental behaviour, several FE modifications and new approaches have been taken. These include: (i) use of a new scaling option for the governing equations which has the effect of equilibrating the stiffness matrices and thus improving their condition; (ii) implementation of several iterative solution techniques such as the iterated penalty and the Uzawa algorithm for the augmented Langrangian to better accommodate the dual role of the pressure; (iii) use of a multistep Newton method to better handle the high non-linearity of the coupled flow/transport problem. Although each of these options (or a combination of them) is able to improve on the quality of FE solution, the most startling amelioration has been gained with option (iii). Use of the latter resulted in very satisfactory modelling of the experimentally observed plumes.

KEY WORDS Thermal plumes Mixed and penalty finite elements Incompressibility Div-stability Scaling Iterated penalty Augmented Langrangian Uzawa algorithm Multistep Newton

* Present address: Department of Mathematics and Statistics, Air Force Institute of Technology, Wright-Patterson AFB, OH 45433, U.S.A.

0271–2091/94/020189–26$18.00

Received 5 June 1992
Revised 17 August 1993

1. INTRODUCTION

Buoyancy-induced plumes in viscous fluids arise in numerous technical,[1] environmental[1] and geological[2,3] disciplines. Many situations in mechanical engineering are governed by the presence of plumes (convective heat transfer[1]). Aerosols in the atmosphere and contaminants in the ocean or in groundwater are often transported in the form of plumes.[1] In recent years there has been increasing evidence of the importance of buoyant heat and mass transport processes in various geological phenomena.[2,3] On a large scale these may include deep-mantle plumes originating at the base of the earth's mantle[2] which manifest themselves surficially in the form of hot spots. Among the latter the island of Hawaii is the most prominent example. On a smaller scale magmatic flows in dykes (volcanic activity) or salt diapirs[2–4] exhibit these processes.

From a fluid-dynamical point of view, many of the above geological flow processes can be characterized as viscous creeping flow with very low Reynolds numbers, i.e. they can in principle be modelled as Stokes flow.[3,5,6] However, such a simple analysis is hampered by the fact that thermally activated fluid flow in the earth's interior is rheologically highly non-linear and in particular has a very strong dependence of its viscosity on the temperature (see References 2 and 7 for reviews). In the earth's mantle, absolute viscosity contrasts μ_{amb}/μ_{int} between the ambient medium and the plume interior are assumed to be of order $O(10^3–10^8)$.[7–10] Such conditions are very difficult to attain in the laboratory[7] and most of the experiments done so far to mimic highly temperature-dependent viscous plumes[7,9–14] have settled for much lower viscosity contrasts. To model such plumes theoretically, asymptotic analytical methods (such as the 'rigid Stokes' limit)[7–9,11,12] have been proposed. However, these analytical techniques often miss important physics of the problem,[7] such as internal fluid circulation in the interior of the plume head (see Figure 1) and diffusional heat and mass loss (and consequently loss of buoyancy) from the plume into the surrounding medium. Depending on the assumptions used in these studies,[7,12–14] several rise laws (plume height h versus time t) in the form $h \sim t^{\beta}$ with β ranging from $\frac{5}{3}$[13] through $\frac{7}{5}$[14] to $\frac{5}{4}$[12] have been derived theoretically or deduced from experiments. Figure 2 shows some typical results of these experimental and analytical studies and of the more recent laboratory investigation of Coulliette.[7] As will be shown in the present paper, the results of his experiments are also well matched by the proposed new finite element analysis.

The discrepancies among the various analytical and experimental studies (Figure 2) and the technical difficulties in performing the latter,[7] but especially their limited applicability to the modelling of more realistic geological plumes, make a full numerical approach highly desirable. Several authors have attempted this by solving the Boussinesq equations (see Section 2) for free convection under the Stokes flow assumption (low Reynolds number and infinite Prandtl number) using finite difference[15] or, more commonly now, finite element methods.[10,16,17] However, these simulations are barely applicable to the modelling of the initialization and growth of a viscous plume such as shown in Figure 1, since they (i) have only incorporated moderate viscosity contrasts and (ii) are more suitable to mimic large-scale mantle convection.

The finite element analysis in the present study has grown out of the need to model experimentally observed plumes[7] (Figure 1) and to predict numerically the appropriate rise laws (Figure 2). The base code used initially has been the general-purpose Bubonov–Galerkin finite element package NACHOS-II[18] for incompressible flow and heat transfer problems. This code is a greatly modified version of the original code NACHOS[19] and has been applied successfully to numerous fluid-mechanical problems.[18,20] NACHOS-II provides a variety of element choices (triangular, eight-point serendipity, nine-point Langrangian) for the velocity and a choice of continuous (Taylor–Hood family) or discontinuous (Crouzeix–Raviart family) elements for the pressure,[21–23] which can be used in conjunction with either a classical mixed (integrated) or a

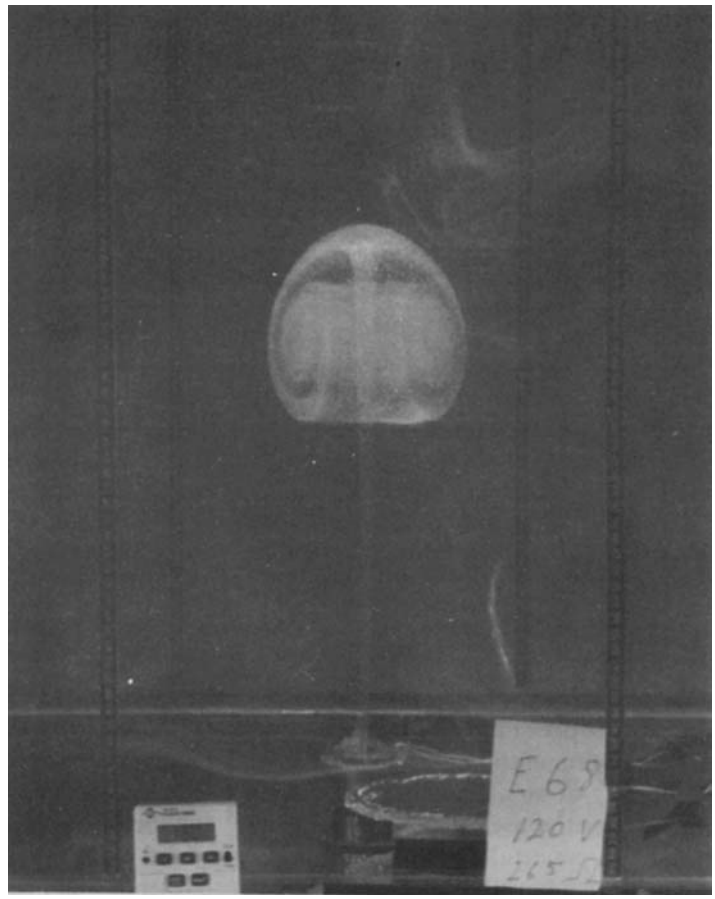

Figure 1. Photograph of a thermal plume in corn syrup with temperature-dependent viscosity.[7] The temperature in the centre of the plume is about 80 °C as compared with $T_{amb} = 0{\cdot}1$ °C in the ambient medium, which results in a viscosity contrast of about $6{\cdot}4 \times 10^4$

penalty formulation. In spite of these options, we have encountered numerical difficulties and eventually breakdowns of the code in the early stages of a transient plume simulation.

In an effort to understand the origins of and develop possible cures for this disastrous behaviour, we have focused on one of the most difficult aspects of finite element analysis of incompressible viscous flow, namely the inherent difficulty of any numerical primitive variable FE method in exactly satisfying the div = 0, incompressibility or mass conservation constraint.[21,23–27] The reasons for this unsatisfactory behaviour which leads to numerical instabilities and eventually to breakdown are manifold and by no means fully understood.[26,27] The most enlightening discussion with regard to this topic is that of Pelletier *et al.*[26] Since these issues are the centrepieces of the present paper, we mention here only the key words: the dual role of the pressure to both satisfy the continuity equation and balance the viscous and buoyancy terms in the momentum equation; the inadequacy of the chosen pressure space (poor choice of elements, locking and non-locking elements) to fulfil the div-stability (LBB) condition; the ill-conditioning of the stiffness matrices; and the inappropriate choice of the penalty parameter.

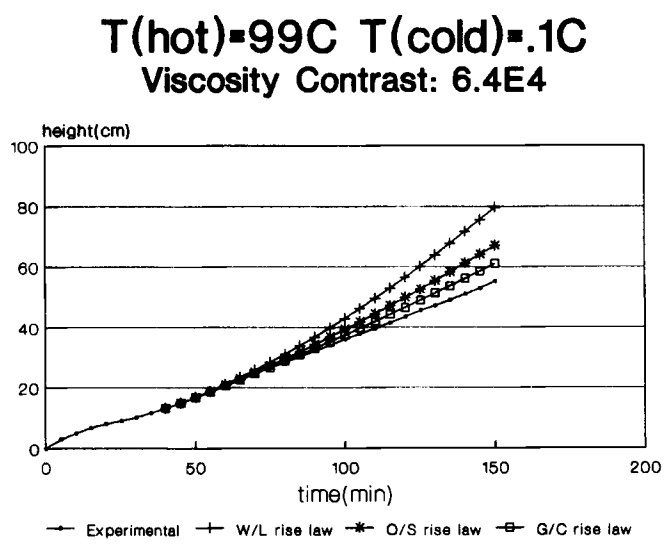

Figure 2. Experimental and analytical rise laws derived for a viscous plume similar to Figure 1 (T_{amb} = 0·1 °C). Notations and references: experimental, Coulliette;[7] *W/L*, Whitehead and Luther;[13] *O/S*, Olson and Singer;[14] *G/C*, Griffiths and Campbell[12]

Pelletier *et al.*[26] also propose some possible cures to better enforce the incompressibility constraint: enlargement of the pressure space through the use of discontinuous pressure elements; scaling to improve the condition of the stiffness matrices; and iterative refinement of the pressure by either an iterated penalty or an augmented Lagrangian method (Uzawa algorithm).[24,28–31] Gunzburger[21] also advocates the use of an iterative penalty method.[21,22] This investigation is essentially an extension and practical application of these proposed cures.

The above issues have so far mostly been investigated for the steady state isothermal Stokes problem in Cartesian co-ordinates and it is not clear how far they apply to the transient FE analysis of a buoyant plume in axisymmetric, cylindrical geometry, whose viscosity is strongly temperature-dependent (Figure 1).[7] The precise modelling of such a plume is the ultimate objective of the present paper. Towards this end we will first diagnose and analyse the possible reasons for the numerical instabilities encountered in the original FE formulation, using the above key words as a guideline. Through computation of the discrete divergence, it will be shown that the failures of the FE method used are indeed related to the poor satisfaction of the div = 0 condition. Following suggestions of Pelletier *et al.*,[26] we then investigate several scaling options for the governing equations and implement some of the iterative methods mentioned above. Finally we present a refined multistep Newton method which accommodates better the high non-linearities in the plume problem. It will be shown that certain combinations of these options are able to remedy most of the fallacies of the original FE formulation and allow us to model the experimentally observed plumes of Coulliette[7] very satisfactorily.

2. MATHEMATICAL FORMULATION OF THE PROBLEM

Governing equations

The physical problem of a thermally buoyant plume is described by the Navier–Stokes equations, the continuity equation for incompressible fluids and the energy equation. Assuming

the usual Boussinesq approximation,[1] these equations are given respectively by

$$\rho \frac{\partial u_i}{\partial t} + \rho u_j \frac{\partial u_i}{\partial x_j} = \rho g_i - \rho g_i \alpha (T - T_{\text{ref}}) + \frac{\partial \tau_{ij}}{\partial x_j}, \tag{1}$$

$$\frac{\partial u_i}{\partial x_i} = 0, \tag{2}$$

$$\rho c_p \frac{\partial T}{\partial t} + \rho c_p u_j \frac{\partial T}{\partial x_j} = -\frac{\partial q_i}{\partial x_i}, \tag{3}$$

where

$$\tau_{ij} = -p\delta_{ij} + \mu\left(\frac{\partial u_i}{\partial x_j} + \frac{\partial u_j}{\partial x_i}\right) \tag{4}$$

is the stress tensor and

$$q_i = -k \frac{\partial T}{\partial x_i} \tag{5}$$

is the heat flux vector. Notations in equations (1)–(5) are: t, the time; u_i, the velocity component in the x_i-co-ordinate direction; p, the non-hydrostatic pressure; T, the temperature; ρ, the density; μ, the dynamic viscosity; c_p, the heat capacity; k, the thermal conductivity; α, the coefficient of thermal expansion; T_{ref}, a reference temperature at which buoyant forces are zero; δ_{ij}, the Kronecker tensor; and $g_i = (0, 0, g)$, the gravitational acceleration.

Non-dimensionalization

It is often convenient to non-dimensionalize equations (1)–(3) to reduce the number of physical parameters and to get some indication of the relative importance of the various terms in the equation. In a theoretical infinite precision computational environment the choice of scaling has no effect on the solution. In finite precision floating point arithmetic, however, a poor choice of scaling may result in unacceptable round-off error.

As will be shown in a later section, the finite element method reduces the continuum equations (1)–(3) to a set of non-linear matrix equations defined on a grid. Pelletier *et al.*[26] observed that a possible reason for the poor satisfaction of the incompressibility constraint in Stokes flow may be ill-conditioning of this matrix system. The large condition numbers may be a consequence of huge differences in the magnitudes of the various elements in the matrices. A key aspect to remember during these discussions is that the major physical processes acting during plume formation and development are the pressure, viscous and buoyant forces. Any valid non-dimensionalization will maintain a balance between the magnitudes of these forces. We will consider how three different scalings affect the relative sizes of the relevant matrix terms. These considerations will lead us to the choice of the appropriate scaling which then will be evaluated in the numerical computations.

Pr–Ra-non-dimensionalization. A widely used scaling technique for thermally convective flow, particularly in geophysical fluid dynamics, is the Prandtl–Rayleigh number form.[1,10,16,17,20] It can be obtained by defining the non-dimensional quantities

$$t' = tD/h^2, \qquad x' = x/h, \qquad u' = uh/D, \qquad p = ph^2/\mu_r D,$$
$$\tau'_{ij} = \tau_{ij} h^2/\mu_r D, \qquad T' = T\Delta T, \qquad \mu' = \mu/\mu_r,$$

where $D = k/\rho c_p$ is the thermal diffusivity, $\Delta T = T - T_{\text{ref}}$, h is a characteristic length scale (taken as either the height of the tank or the size of the heater plate) and μ_r is the reference viscosity of the ambient fluid. This puts equations (1)—after eliminating the ground state hydrostatic pressure ρg_i—and (3) in the form (primes are dropped)

$$\frac{1}{Pr}\left(\frac{\partial u_i}{\partial t} + u_j \frac{\partial u_i}{\partial x_j}\right) = Ra(T - T_{\text{ref}})\mathbf{e}_z + \frac{\partial \tau_{ij}}{\partial x_j}, \tag{6a}$$

$$\frac{\partial T}{\partial t} + u_j \frac{\partial T}{\partial x_j} = \frac{\partial^2 T}{\partial x_i^2}, \tag{7a}$$

where $Ra = \alpha g \Delta T h^3/\nu_r D$ is the Rayleigh number, $Pr = \nu_r/D$ is the Prandtl number, $\nu_r = \mu_r/\rho$ is the kinematic viscosity and $\mathbf{e}_z$ is the unit vector in the vertical direction.

Using the tank height as the length scale h in this formulation for a plume experiment with $T_{\text{amb}} = 0{\cdot}1\ ^\circ\text{C}$ (see Figure 1) results in $Ra = 6{\cdot}5 \times 10^6$ (see Table I). Such a large value of Ra places too much weight on the buoyancy term in the momentum equation (6a). The result of this overemphasis on buoyancy is an ill-conditioned system whose velocity field does not satisfy the continuity equation (2). We will discuss numerical examples of this scaling in a later section.

Pr–$Gr^{1/2}$-non-dimensionalization. This scaling technique is more commonly used in engineering fluid mechanics[32–35] and is obtained by defining the non-dimensional quantities

$$t' = tu_0/h, \qquad x' = x/h, \qquad u' = u/u_0, \qquad p' = p/\rho u_0^2,$$

$$\tau'_{ij} = \tau_{ij}/\rho u_0^2, \qquad T' = T\Delta T, \qquad \mu' = \mu/\mu_r,$$

where $u_0 = (g\alpha\Delta T h)^{1/2}$ is another characteristic velocity scale. This results in

$$Gr^{1/2}\left(\frac{\partial u_i}{\partial t} + u_j \frac{\partial u_i}{\partial x_j}\right) = Gr^{1/2}(T - T_{\text{ref}})\mathbf{e}_z + \frac{\partial \tau_{ij}}{\partial x_j}, \tag{6b}$$

$$PrGr^{1/2}\left(\frac{\partial T}{\partial t} + u_j \frac{\partial T}{\partial x_j}\right) = \frac{\partial^2 T}{\partial x_i^2}, \tag{7b}$$

where $Gr = Ra/Pr = \alpha g \Delta T h^3/\nu_r^2$ is the Grashof number.

This scaling is closer to maintaining the proper balance between viscous forces and buoyant forces for the plume problem. This proper balance, however, is due more to good fortune than to proper scaling based on physical considerations, since the Grashof number is small for the cases under consideration here (e.g. $Gr = 3 \times 10^{-3}$ for $T_{\text{amb}} = 0{\cdot}1\ ^\circ\text{C}$; see Table I). For cases with a very large Grashof number ($Ra \gg Pr$) this scaling would also place too much emphasis on the buoyancy.

Pr-non-dimensionalization. In the following we present a new scaling option which has been found to be very advantageous in the present thermal plume problem, particularly for high viscosity contrasts. In this approach we non-dimensionalize the governing equations using

$$t' = tu_0/L, \qquad x' = x/L, \qquad u' = u/u_0, \qquad p' = p/\rho g \alpha \Delta T L,$$

$$\tau'_{ij} = \tau_{ij}/\rho g \alpha \Delta T L, \qquad T' = T/\Delta T, \qquad \mu' = \mu/\mu_r,$$

where

$$L = (\mu_r D/\rho g \alpha \Delta T)^{1/3}, \qquad u_0 = D/L, \qquad \Delta T = T_{\text{heater}} - T_{\text{amb}}, \qquad \mu_r = \mu_{\text{amb}}.$$

Substitution of these quantities in the governing equations (1) and (3) results in

$$\frac{1}{Pr}\left(\frac{\partial u_i}{\partial t} + u_j \frac{\partial u_i}{\partial x_j}\right) = (T - T_{\text{ref}})\mathbf{e}_z + \frac{\partial \tau_{ij}}{\partial x_j}, \tag{6c}$$

$$\frac{\partial T}{\partial t} + u_j \frac{\partial T}{\partial x_j} = \frac{\partial^2 T}{\partial x_i^2}. \tag{7c}$$

We call this the Prandtl number non-dimensionalization approach since only Pr occurs in the equations. However, a second parameter does appear (though not explicitly), namely the 'variable' length scale L defined as above. One notes from the definition of L that the latter has the effect of normalizing the Rayleigh number to $Ra = 1$. This is done over the ΔT-term, i.e., because the heater temperature T_{heater} is kept constant in the experiments, over the ambient temperature T_{amb}. In order to restore the physical balance between the buoyant and the pressure plus viscous forces, the whole set of equations is now non-dimensionalized with L computed in this way. This means that unlike in the earlier two scaling options, where L is constant and equal to either the height h of the container or the size of the heater, L will now be dependent on ΔT. As such, the strength of the buoyancy, which has formerly been described through Ra, is now expressed in terms of L. Hence the equations are solved in a rectangular domain (Figure 3) whose vertical dimension is to be computed from $h' = h/L$ and which in turn is dependent on the ambient temperature T_{amb} of the plume experiment modelled. For example, for $T_{\text{amb}} = 0{\cdot}1$ °C, Table I lists a value $L = 1{\cdot}58$ cm. With the vertical height h of 69 cm for the real tank (see following section), this results in a scaled height h' of 43·7 cm for the computational domain. Table I shows that compared with the range of variation for Ra and Gr, which extends over several orders of magnitude, that of L is significantly less, which is why this scaling option behaves better in the numerical computations. In fact, as will be shown in the numerical computations, a better algebraic conditioning of the discretized FE equations results from this scaling option.

Viscosity law

Equations (1) and (3) are coupled by an equation of state for the viscosity μ as a function of temperature T. For corn syrup the viscosity experiments of Coulliette[7] result in a best-fitting law that can be written in the form

$$\mu(T) = 10^{(A + B/T + C/T^2)}, \tag{8}$$

where A, B and C were determined via regression as 20·6, −14,990 and 3,076,200 respectively, $\mu(T)$ is in $(Pa\ s) \times 10^{-3}$ and T is in kelvins. Depending on the temperature differences ΔT between the plume interior and ambient medium, which range between about 50 and 100 °C in the experiments, equation (8) results in viscosity contrasts $\mu_{\text{amb}}/\mu_{\text{int}}$ of order $O(10^2$–$10^7)$.

The values of the other physical parameters used in the computations are $T_{\text{heater}} = 100$ °C, $D = 2{\cdot}2 \times 10^{-3}$ cm^2 s^{-1}, $c_p = 0{\cdot}7$ cal g^{-1} K^{-1} (both are assumed independent of temperature) and $\alpha = 3{\cdot}5 \times 10^{-4}$ K^{-1}. Table I lists the values for the temperature-dependent parameters ρ and μ_r as well as the values for Pr, Gr, Ra and the length scale L obtained with the ambient temperatures T_{amb} of 25, 0·1 and −26·1 °C used for the three model experiments.

Table I. Numerical values for the density ρ, the reference dynamic viscosity μ_r, the Prandtl number Pr, the Grashob number Gr, the Rayleigh number Ra and the length scale L (used in the new Pr-scaling) for the three model experiments with ambient temperatures T_{amb} of 25, 0·1 and −26·1 °C

T_{amb}(°C)	ρ(g cm^{-3})	μ_r(Pa s)	Pr	Gr	Ra	L(cm)
25·0	1·42	84·9	$2{\cdot}7 \times 10^{5}$	26·0	$6{\cdot}5 \times 10^{6}$	0·37
0·1	1·43	$8{\cdot}7 \times 10^{3}$	$2{\cdot}8 \times 10^{7}$	$3{\cdot}0 \times 10^{-3}$	$8{\cdot}4 \times 10^{4}$	1·58
−26·1	1·45	$2{\cdot}1 \times 10^{7}$	$6{\cdot}5 \times 10^{10}$	$5{\cdot}5 \times 10^{-10}$	36·0	19·43

Geometry and boundary conditions

Boundary conditions have been chosen so as to model the rise of an axisymmetric buoyant thermal plume above a circular heater plate in an open rectangular container (Figure 3) of dimensions 0·79 × 0·79 × 0·69 m^3 (see Reference 7 for experimental details). Thus the computations are performed in an axisymmetric cylindrical co-ordinate system ($r = x_1$, $z = x_2$), employing the appropriately reformulated form of the governing equations (6) and (7) for such a

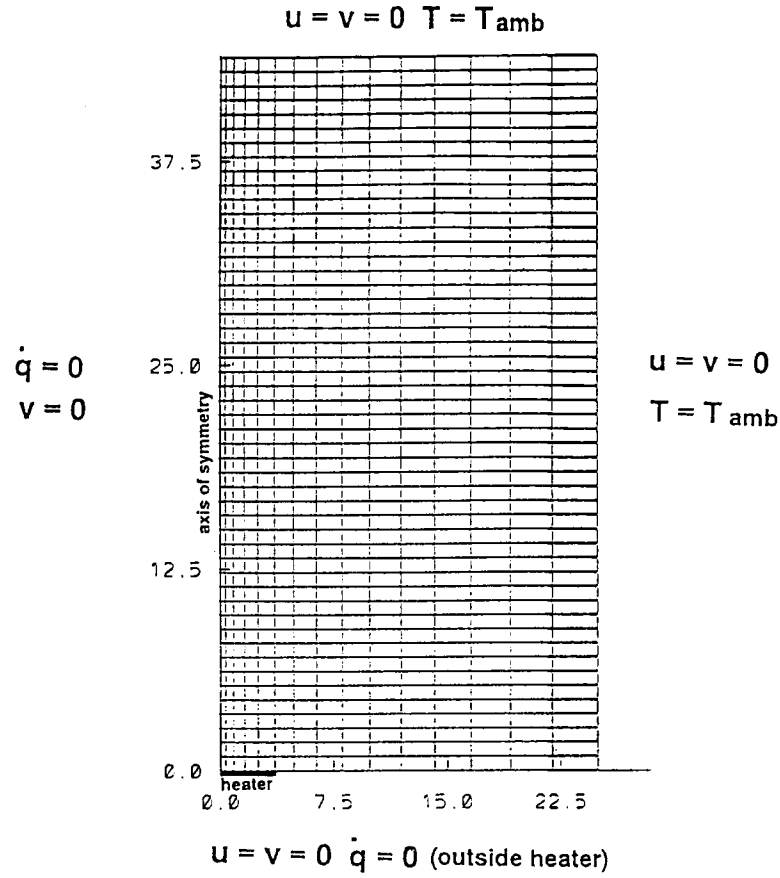

Figure 3. Sketch of geometry, grid and boundary conditions used in the computations

system.[7] This means for the $r = x_1$-component in the momentum equation (6) an additional term $-\mu u_1/r^2$ in the viscous term and for the energy equation (7) a term $(1/r)\partial T/\partial r$ in the diffusion term. As will be shown in the numerical simulations by comparisons with computations in an ordinary (x, y) Cartesian co-ordinate system, these r-dependent terms lead to significant computational difficulties in the axisymmetric case and are the reason why the latter is intrinsically much harder to solve numerically than the Cartesian case.

The centre of the plume is located at $x_1 = 0$ and forms the symmetry boundary, i.e. $u_1 = q_1 = 0$. All the other boundaries are assumed to be no-slip boundaries ($u_1 = u_2 = 0$). The temperature is assumed to be the ambient temperature on the top and side boundaries, i.e. a Dirichlet boundary condition $T = T_{amb}$ is imposed. Along the bottom boundary ($x_2 = 0$), perfect insulation ($q_2 = 0$) is assumed, excluding the heater where a Neumann boundary condition for the heat flux q_i (calculated from the adjustable electric power of the heater) is imposed. In some of the computations this heat flux was specified as being time-dependent. Such an approach not only better mimics the experimental conditions but also turned out to be beneficial for filtering out numerical instabilities which occurred occasionally during the initial start-up phase of a transient FE simulation. Figure 3 illustrates the geometry, the named boundary conditions and a typical FE mesh. The latter is strongly refined towards the plume axis ($r = 0$) to accommodate the strong horizontal velocity and temperature gradients occurring there. Details of the choice of the FE grid and its implication on the numerical solution will be presented later. We emphasize again that in the case of the new Pr-scaling option the effective vertical dimension of the computational domain is computed from the length scale L as listed in Table I.

3. FINITE ELEMENT METHOD

Galerkin formulation for mixed and penalty methods

The core FE code employed in the present study is the general-purpose 2D FE package NACHOS-II,[18] which is based on a classical (Bubonov) Galerkin weak formulation[21,22] for equations (1)–(3). It can be used either as a mixed (integrated) (u, v, p)-method or as a penalty method. For an appreciation of the limitations of these techniques in solving plume flow and of the proposed modifications, their theoretical foundations will be presented in the following (see Reference 18 for details).

A discretization of the domain $\Omega \subset \mathbb{R}^2$ in finite elements Ω_h is assumed. The finite element space for both the velocity $\mathbf{u} = (u, v)^T$ and the temperature $\mathbf{T}$ is defined by $\mathbf{V}^h \subset H_0^1(\Omega)$ and that for the pressure p by $P^h \subset L_0^2(\Omega)$, where $H_0^1(\Omega)$ is the Sobolev space with one square integrable derivative and whose elements vanish on the boundary Γ of Ω, and $L_0^2(\Omega)$ is the space of square integrable functions having zero mean over Ω.[21]

Using the test functions $\mathbf{v}^h \equiv \mathbf{T}^h \in \mathbf{V}^h$ in equations (1) and (3) and $q^h \in P^h$ in equation (2), one obtains the discrete Galerkin equations (weak formulation)

$$\frac{\partial m\langle \mathbf{u}^h, \mathbf{v}^h\rangle}{\partial t} + a\langle \mathbf{u}^h, \mathbf{v}^h\rangle + c\langle \mathbf{u}^h, \mathbf{u}^h, \mathbf{v}^h\rangle + b\langle \mathbf{v}^h, p^h\rangle = \langle \mathbf{f}_u, \mathbf{v}^h\rangle, \tag{9}$$

$$b\langle \mathbf{u}^h, q^h\rangle = 0, \tag{10}$$

$$\frac{\partial m_T\langle \mathbf{T}^h, \mathbf{v}^h\rangle}{\partial t} + a_T\langle \mathbf{T}^h, \mathbf{v}^h\rangle + c_T\langle \mathbf{T}^h, \mathbf{T}^h, \mathbf{v}^h\rangle = \langle \mathbf{f}_T, \mathbf{v}^h\rangle, \tag{11}$$

where $m\langle\cdot,\cdot\rangle$, $a\langle\cdot,\cdot\rangle$, $b\langle\cdot,\cdot\rangle$ and $c\langle\cdot,\cdot\rangle$ are bilinear forms[21] describing the volume integrals for the time derivatives (mass matrix), the diffusion, the pressure and the incompressibility

term (dual role of the pressure) and the convective terms respectively; $\mathbf{f}_u$ and $\mathbf{f}_T$ include the buoyancy term and heat source terms respectively and terms due to natural boundary conditions on Γ arising from the application of Green's theorem to the volume integrals. Equations (9) and (10) describe the Galerkin method for the Navier–Stokes (NS) equations in the general mixed or integrated velocity–pressure ($\mathbf{u}$, p) formulation where the incompressibility (divergence-free) constraint (10) is explicitly enforced by solving equations (9) and (10) simultaneously.

The second FE option to be applied is the penalty method, which is becoming more widely used in FE computations.[21,22] Here the incompressibility term (10) is penalized by the pressure in the form

$$b\langle \mathbf{u}^h, q^h \rangle = \varepsilon \langle p, q^h \rangle, \tag{12}$$

where $\varepsilon \ll 1$ is an arbitrary (see discussion in the next section) penalty parameter. Equation (12) provides an explicit expression for the pressure. Substituting it in the discretized NS equation (9) eliminates the pressure from the problem and so reduces the total number of degrees of freedom of the problem.

To get the discrete matrix version of the problem in the two formulations, local interpolating functions for $\mathbf{u} = (u, v)^T$, p and T are introduced on the element level. Thus one has $\mathbf{u} = \mathbf{v}^{h^T} u_i$, $\mathbf{p} = \mathbf{q}^{h^T} p_i$ and $\mathbf{T} = \mathbf{v}^{h^T} T_i$, where u_i, p_i and T_i are the corresponding nodal values of the elements chosen. Substituting these expressions in equations (9)–(11), one obtains the local or, after elementwise assembly, global matrix system

$$\begin{pmatrix} \mathbf{M} & 0 & 0 \\ 0 & 0 & 0 \\ 0 & 0 & \mathbf{N} \end{pmatrix} \begin{pmatrix} \partial \mathbf{u}/\partial t \\ \partial \mathbf{p}/\partial t \\ \partial \mathbf{T}/\partial t \end{pmatrix} \begin{pmatrix} \mathbf{C}(\mathbf{u}) + \mathbf{K}(\mathbf{u}, \mathbf{T}) & -\mathbf{Q} & \mathbf{B}(\mathbf{T}) \\ -\mathbf{Q}^T & 0 & 0 \\ \mathbf{0} & 0 & \mathbf{D}(\mathbf{u}) + \mathbf{L}(\mathbf{T}) \end{pmatrix} \begin{pmatrix} \mathbf{u} \\ \mathbf{p} \\ \mathbf{T} \end{pmatrix} = \begin{pmatrix} \mathbf{F}(\mathbf{T}) \\ \mathbf{0} \\ \mathbf{G}(\mathbf{T}, \mathbf{u}) \end{pmatrix} \tag{13}$$

for the integrated method and

$$\begin{pmatrix} \mathbf{M} & 0 \\ 0 & \mathbf{N} \end{pmatrix} \begin{pmatrix} \partial \mathbf{u}/\partial t \\ \partial \mathbf{T}/\partial t \end{pmatrix} \begin{pmatrix} \mathbf{C}(\mathbf{u}) + \mathbf{K}(\mathbf{u}, \mathbf{T}) + (1/\varepsilon)\mathbf{Q}\mathbf{M}_p^{-1}\mathbf{Q}^T & \mathbf{B}(\mathbf{T}) \\ \mathbf{0} & \mathbf{D}(\mathbf{u}) + \mathbf{L}(\mathbf{T}) \end{pmatrix} \begin{pmatrix} \mathbf{u} \\ \mathbf{T} \end{pmatrix} = \begin{pmatrix} \mathbf{F}(\mathbf{T}) \\ \mathbf{G}(\mathbf{T}, \mathbf{u}) \end{pmatrix} \tag{14}$$

for the penalty method. Notations are: $\mathbf{M}$, $\mathbf{M}_p$ and $\mathbf{N}$, the mass matrices for velocity, pressure and temperature respectively; $\mathbf{C}$ and $\mathbf{D}$, the advection matrices for velocity and temperature respectively; $\mathbf{K}$ and $\mathbf{L}$, the diffusion matrices for velocity and temperature respectively; $\mathbf{Q}$ and $\mathbf{Q}^T$, the matrices associated with the gradient operator; $\mathbf{B}$, the buoyancy matrix; $\mathbf{F}(\mathbf{T})$ and $\mathbf{G}(\mathbf{T}, \mathbf{u})$, the forcing functions (source terms) and natural boundary conditions in the momentum and energy equations respectively.

Time integration and matrix solution

The Galerkin equations in both the integrated (equation (13)) and penalty (equation (14)) formulations can be formally written as a non-linear system of ODEs in time:

$$\bar{\mathbf{M}} \frac{\partial \bar{\mathbf{V}}}{\partial t} + \bar{\mathbf{K}}(\mathbf{u}, \mathbf{T})\bar{\mathbf{V}} = \bar{\mathbf{F}}(\mathbf{u}, \mathbf{T}), \tag{15}$$

where $\bar{\mathbf{V}} = (\mathbf{u}, \mathbf{p}, \mathbf{T})^T$. For the time integration of equation (13) an explicit–implicit predictor–corrector method is employed in the NACHOS-II code.[18] A frontal method (Gaussian elimination based on element ordering) is used for the solution of the matrix systems arising in the implicit time discretization of equation (13) or (14). Both a first-order forward Euler predictor and backward Euler corrector and a second-order Adams–Bashforth predictor and trapezoidal

(Crank–Nicholson) corrector are available. In spite of the increased accuracy of the second-order methods and the possible use of larger time steps, we have found it extremely helpful to take advantage of the strong damping characteristics of the first-order Euler method[22] to filter out solution instabilities which occur often in the initial stages of a transient plume simulation.

Note that in the formulations of equations (13) and (14) the temperature T in the energy equation is implicitely coupled via the buoyancy term in the momentum equation to both the velocity $\mathbf{u}$ and the pressure p. This is unlike many other FE or FD techniques for coupled flow/heat problems (free convection),[31] such as in the predecessor of NACHOS-II, NACHOS,[19] where the momentum and energy equations are solved consecutively. Such a coupled approach should in principle result in a better representation of temperature and velocity at each time step, but at the expense of increasing the number of degrees of freedom of the problem. Moreover, as will be discussed later, there is some evidence that the implicit coupling of $\mathbf{u}$ and T might accentuate the overall non-linearity of the plume problem.

Theoretical and practical difficulties associated with the divergence-free condition in mixed and penalty methods

The success of an FE analysis of the coupled momentum/energy problem by either the mixed or the penalty method is directly related to the solvability of the global matrix systems (13) and (14) respectively and the uniqueness of the solutions obtained for $\mathbf{u} = (u, v)^{\mathrm{T}}$, p and T. Nearly all theoretical and practical studies with regard to this issue have been performed for the isothermal, pure Navier–Stokes problem or, more precisely, the linear, steady state, elliptic Stokes problem (low-Reynolds-number creeping flow.[21,24–27] Although our numerical simulations indeed show that the results of these investigations cannot be totally generalized to the modelling of a (highly non-linear) viscous plume, they provide valuable guidelines on how to tackle the problem successfully. In the following we therefore discuss some of these issues with regard only to the isothermal, steady state Stokes problem.

For convenience we extract the relevant matrices for the Stokes problem from equations (13) and (14) to obtain

$$\begin{pmatrix} \mathbf{K} & -\mathbf{Q} \\ -\mathbf{Q}^{\mathrm{T}} & \mathbf{0} \end{pmatrix} \begin{pmatrix} \mathbf{u} \\ \mathbf{p} \end{pmatrix} = \begin{pmatrix} \mathbf{f} \\ \mathbf{0} \end{pmatrix} \tag{16}$$

for the mixed (integrated) method and

$$[\mathbf{K} + (1/\varepsilon)\mathbf{Q}\mathbf{M}_p^{-1}\mathbf{Q}^{\mathrm{T}}]\mathbf{u} = \mathbf{f}, \tag{17}$$

$$\mathbf{Q}^{\mathrm{T}}\mathbf{u} + \varepsilon\mathbf{M}_p\mathbf{p} = 0 \tag{18}$$

for the penalty method.

The solvability of the system (16) is closely related to the concepts of the divergence-free (div = 0 or incompressibility) constraint $b\langle \mathbf{u}^h, q^h \rangle = 0$ (equation (10)) (or its discrete matrix form $\mathbf{Q}^{\mathrm{T}}\mathbf{u} = 0$) and of the pressure modes of the system.[25,27] The pressure $q^h(p)$ plays a dual role in both enforcing the div = 0 condition and balancing the momentum forces in the Stokes equation. This can be clearly seen when viewing the incompressible Stokes problem as a constrained minimization problem[21,22] with a discrete Lagrangian L in the form

$$L = \tfrac{1}{2}\mathbf{u}^{\mathrm{T}}\mathbf{K}\mathbf{u} - \mathbf{u}^{\mathrm{T}}\mathbf{f} + p\mathbf{Q}^{\mathrm{T}}\mathbf{u} \tag{19}$$

where p in the last term acts as a Lagrangian multiplier to enforce the div = 0 condition. Minimization of equation (19) results directly in the matrix system (16).

On account of the **0** in the lower right element of the global Stokes matrix (16) in the mixed method, the matrix is singular, which reflects the well-known fact that the pressure in the momentum equation can only be determined up to a constant. Because of this singularity, the homogeneous system (assuming the right-hand side $\mathbf{f} \equiv \mathbf{0}$) has non-trivial pressure solutions $p \neq 0$, which are the so-called pressure modes of the system (16). The understanding of the theoretical and numerical role of these pressure modes in FE solutions is one of the most intriguing issues in FE analysis[21–27] and is by no means complete. As long as the pressure mode is just a constant, the solvability of the inhomogeneous system (16) is guaranteed via the Fredholm alternative and the discrete divergence-free condition $\mathbf{Q}^T\mathbf{u} = 0$ is globally satisfied. Of more concern are the pressure modes $p \neq$ constant, the so-called spurious modes. Since they correspond to zero forcing, they have no physical meaning. Then, again via the Fredholm alternative, the inhomogeneous Stokes equations (16) have a non-trivial solution only if the right-hand side of equation (16) is orthogonal to a pressure mode. In the presence of spurious modes this might not be the case for arbitrary boundary conditions and the solvability of equation (16) might be impaired. Moreover, it can be shown[25] that a spurious pressure mode $p \neq$ constant reduces the effective number of incompressibility constraints by one, i.e. produces a dual velocity field which is marginally compressible. Thus the presence of the spurious pressure modes is closely related to the violation of the div = 0 condition. This has also been supported by the 'no-flow tests' of Gresho *et al.*[36] and Pelletier *et al.*[26]

Since the form and nature of the Stokes matrix in equation (16) depend on the choice of the trial and interpolation spaces $\mathbf{V}^h$ and P^h for the velocity $\mathbf{u}$ and the pressure p respectively, the selection of an appropriate element is an important consideration. The generally accepted requirement for an eligible element is that the interpolation functions for the pressure be at least one order less than those for the velocity.[21,22] Also, the velocity functions must be continuously differentiable in each element and continuous in the whole domain, whereas the pressure functions may be continuous (Taylor–Hood family) or discontinuous (Crouzeix–Raviart family) between elements. Other than that, the modeller is still faced with the above considerations of the pressure modes and of the div = 0 condition.

Because a rigorous mathematical proof of the theoretical performance of a particular finite element for the incompressible Stokes problem (16), let alone the full Navier–Stokes problem, is still lacking, often some more heuristic arguments provide help. Among these the concepts of incompressibility constraint counting and the constraint ratio r have been found useful.[23] The constraint ratio is defined as $r = n_{eq}/n_c$, where n_{eq} is the total number of velocity equations after boundary conditions have been imposed and n_c is the total number of incompressibility constraints as specified by the pressure nodes. For many cases with a two-dimensional mesh the optimal value for r is $r = 2$, in which case the div = 0 condition is sufficiently enforced while still allowing a sufficient degree of freedom for the displacements (velocities). Values of $r < 2$ ($r > 2$) indicate too many (too few) incompressibility constraints. In the extreme case $r < 1$ so-called 'locking' of the mesh occurs and only the trivial (locked) solution $\mathbf{u} = 0$ is obtained. While constraint counting has no theoretical support, it is often helpful in comparing elements for many flow problems.

Another related but rather poorly understood aspect in practice is the Ladyzhenskaya–Babuska–Brebbi (LBB), inf-sup or div-stability condition[21,23,24] of a particular class of elements, defined as

$$\sup \frac{b\langle \mathbf{v}^h, q^h \rangle}{|\mathbf{v}^h|_1} \geq \tau \|q^h\|_0, \quad \mathbf{v}^h \in \mathbf{V}_0^h, \quad q^h \in P^h, \tag{20}$$

where $\tau > 0$ is arbitrary. LBB essentially ensures that when the size h of the elements goes to zero,

the discrete computed velocity of the Stokes problem is truly solenoidal, i.e. the div = 0 condition is satisfied. Moreover, LBB guarantees that the divergence term $b\langle \mathbf{v}^h, q^h \rangle$ in equation (20) goes to zero faster than the velocity, so that mesh locking will not occur. The other important consequence of LBB is that convergence rates for the sum of the velocity and pressure can be exactly estimated in the space $\mathbf{V}_0^h$, whereas if LBB is not satisfied, this is only possible in the space $\mathbf{Z}$ of the divergence-free functions.[21] Although LBB guarantees optimal convergence of the finite element solution, it is only a sufficient and not a necessary condition, i.e. optimal convergence may be achieved in some instances without LBB being satisfied.[37] Therefore the LBB condition appears to be more of theoretical than of practical value.[21,26] As pointed out by Pelletier *et al.*,[26] the LBB condition does provide information on the above issue of the spurious pressure modes but not on the enforcement of the div = 0 condition. A typical example is the notorious bilinear velocity, constant pressure (Q_1–P_0) element, which violates LBB, conserves mass ($b\langle \mathbf{v}^h, q^h \rangle = 0$) and has an optimal value of the above constraint ratio $r = 2$, but shows the disastrous checkerboard mode for the pressure.[21,27] Nor does the LBB condition define an optimal value of r, so that an element with $r > 2$ may satisfy the LBB condition yet not enforce the incompressibility condition adequately. This is illustrated in Table II, where the constraint ratio r and the div-stability of the elements available in NACHOS-II are summarized. On the basis of the LBB condition, the nine-point quadrilateral Langrangian element QUAD9 with biquadratic velocity interpolation appears theoretically to be preferable over the eight-point quadrilateral element QUAD8 with discontinuous pressure approximation which does not satisfy LBB. However, the situation is less clear for the eight-point serendipity element QUAD8 with continuous pressure, since this one satisfies LBB too. Since the rate of convergence derived for all these elements is identical,[24] none of them appears to have any theoretical advantage. On the other hand, the constraint ratio r for the QUAD8 element is closer to the optimal value $r = 2$ than that for the QUAD9 element and therefore the incompressibility constraint

Table II. Constraint count r, div-stability (LBB) and discrete divergence DDIV obtained with the mixed method or the penalty method ($\varepsilon = 10^{-12}$) and the three scaling options used (*Pr*–*Ra*, equations (6a) and (7a); *Pr*–$Gr^{1/2}$, equations (6b) and (7b); new *Pr*-scaling, equations (6c) and (7c)) for the axisymmetric plume model with $T_{amb} = 0{\cdot}1$ °C for several element types available in NACHOS-II. Notations are: QUAD8, the eight-point quadrilateral serendipity element with incomplete biquadratic velocity interpolation; QUAD9, the nine-point quadrilateral Lagrangian element with complete biquadratic velocity interpolation; cont. *p*, continuous bilinear pressure approximation (Taylor–Hood); disc. *p*, discontinuous bilinear pressure approximation (Crouzeix–Raviart). The last column depicts reference values for DDIV obtained in a Cartesian co-ordinate system

				Discrete divergence (DDIV)			
				Axisymmetric			Cartesian
Element	r	LBB?	Method	*Pr*–*Ra*	*Pr*–$Gr^{1/2}$	*Pr* (new)	*Pr* (new)
QUAD8, disc. *p*	2	No	Mixed	10^{-10}	10^{-12}	10^{-13}	10^{-14}
			Penalty	10^{-6}	10^{-5}	10^{-11}	10^{-12}
QUAD8, cont. *p*	6	Yes	Mixed	10^{-6}	10^{-3}	10^{-7}	10^{-8}
QUAD9, disc. *p*	$2\frac{2}{3}$	Yes	Mixed	10^{-9}	10^{-12}	10^{-12}	10^{-14}
			Penalty	10^{-5}	10^{-5}	10^{-11}	10^{-12}
QUAD9, cont. *p*	8	Yes	Mixed	10^{-6}	10^{-3}	10^{-7}	10^{-8}

should theoretically be better enforced by QUAD8 than by QUAD9. Using the same arguments, the discontinuous pressure approximation should be more effective for modelling the divergence-free condition than the continuous pressure approximation. This has been demonstrated for the 'no-flow' steady state Boussinesq test problem of Gresho *et al.*[36] by Pelletier *et al.*[26] It has been explained by the latter authors in terms of the dual role of pressure in both enforcing the continuity equation and balancing the viscous and buoyancy terms in the momentum equation. To be able to fulfil both these requirements, the pressure space has to be sufficiently rich. This is better guaranteed by the discontinuous (Q_2–P_1) than by the continuous (Q_2–Q_1) pressure element.

Many of the above considerations also hold for the penalty method. Here the discrete divergence-free constaint $\mathbf{Q}^T\mathbf{u} = 0$ is enforced by means of the penalty function P in the form

$$P = \tfrac{1}{2}\mathbf{K}\mathbf{u}^2 - \mathbf{u}^T\mathbf{f} + \tfrac{1}{2}\lambda\mathbf{u}^T\mathbf{Q}^T\mathbf{Q}\mathbf{u}, \tag{21}$$

where $\lambda = 1/\varepsilon$. Minimization of equation (21) provides equations (17) and (18). It follows that the smaller ε is, the better the incompressibility is enforced. However, too small an ε will deteriorate the condition of the total stiffness matrix in equation (17).

4. THE DISCRETE DIVERGENCE

As suggested by the discussion in the previous section, most of the numerical intricacies in the FE modelling of incompressible Stokes flow are related to the satisfaction of the continuity equation or the incompressibility constraint. This has been clearly supported by the FE simulations of Stokes flow by Pelletier *et al.*,[26] who demonstrate that the FE solutions become unreliable and physically spurious whenever the numerically computed 'discrete divergence'

$$\mathrm{DDIV} = \max_{nel} |\mathbf{Q}^T\mathbf{u}^h| \tag{22}$$

becomes too large. In equation (22) $\mathbf{Q}^T$ is the matrix equivalent of the divergence operator (see equation (13)), $\mathbf{u}^h$ is the computed velocity vector on an individual element and the maximum is taken over all elements of the mesh (*nel*). Pelletier *et al.*[26] regard the discrete divergence DDIV as a powerful diagnostic tool for the evaluation of an FE solution and recommend that it be computed in any FE simulation. FEM theory predicts that the discrete divergence should be of the order of machine zero (10^{-14} for the Cray-YMP used for the calculations) for the integrated FEM and of order $O(\varepsilon)$ for the penalty FEM for a solution demonstrating acceptable mass conservation. In the following tests of the mixed and penalty FEMs, DDIV would generally increase by one or two orders of magnitude before a problem, either in the form of a matrix ill-conditioning error or an unrealistic value of velocity or temperature, occurred. Experience has shown that the change in DDIV is a conservative diagnostic, i.e. an increase in discrete divergence does not always signal a problem. Nevertheless DDIV has been found to be a valuable indicator of which method and element are best suited for modelling the plume problem and has guided us in the development and evaluation of some of the new techniques proposed in later sections.

5. NUMERICAL SIMULATIONS BY MEANS OF THE ORIGINAL NACHOS-II CODE

From this point on we will focus on our goal of the finite element modelling of buoyant creeping plumes with a strong temperature dependence of the viscosity (see Figure 1). In the following sections we report results of simulations using some of the solution and element options of the original NACHOS-II code.

Effects of element choice

From the earlier discussion of the theoretical performance of the various elements we concluded, on the basis of the div-stability condition and the heuristic argument of the constraint count, that elements with discontinuous (disc.) pressure interpolation functions (Crouzeix–Raviart) have better divergence constraint properties than those where the pressure is continuous (cont.) across elements (Taylor–Hood) (see Table II). The discrete divergence calculations using the mixed method confirm these characteristics (Table II) on a sample grid for the plume model with $T_{amb} = 0{\cdot}1$ °C. For both the QUAD8 and QUAD9 elements the disc. *p*-version has a smaller discrete divergence DDIV than the cont. *p*-element. Note that the DDIV values for the QUAD8 and QUAD9 elements are comparable. The heuristic constraint count argument favours QUAD8 (and it has a slightly smaller DDIV) and the theoretical LBB condition favours QUAD9 (particularly for mesh refinement). These and similar results for other ambient experimental conditions (viscosity contrasts) favour the use of the disc. *p*-element in plume FE modelling.

Nevertheless, in spite of the minimal values of DDIV obtained with the disc. *p*-elements for the sample computations of Table II, DDIV would often grow as the plume solution progressed in time. Gradual growth was expected owing to the larger values of the velocity **u** and the accumulation of round-off errors. However, often DDIV would remain small for a period of time, then increase sharply (usually by at least two orders of magnitude) before an error occurred. Such a rapid growth served as a good indicator that the solution would encounter an ill-conditioned matrix error or that the computed temperature and velocity would increase to unrealistically large values.

The integrated (mixed) method

The disastrous behaviour of the discrete divergence DDIV obtained for the plume model with $T_{amb} = 0{\cdot}1$ °C using the mixed method and the QUAD8, disc. *p*-element is illustrated in Figure 4 (top). Following the large increase in DDIV at time steps 10 (for *Pr–Ra*-scaling) and 500 (for the new scaling, see below), the temperature rose to an unrealistically large value.

The penalty method

As mentioned earlier, the selection of the appropriate penalty parameter ε is crucial in the penalty method.[21,26] Too small an ε will ill-condition the problem and too large an ε will introduce too much compressibility. For example, for plume simulations with $T_{amb} = 25$ °C and using the QUAD8, disc. *p*-element, the following values (ε, DDIV) were obtained—$(10^{-15}, \sim 10^{-8})$, $(10^{-14}, \sim 10^{-5})$ and $(10^{-13}, \sim 10^{-3})$—illustrating the large sensitivity of DDIV to ε. The approach used to determine the most appropriate ε was to make several sample runs and observe which number gave the best DDIV behaviour. As usual, early time steps in the simulation showed great promise, but the DDIV would increase sharply at some stage later and the solution soon encountered an ill-conditioning error. By using a fine mesh and varying the penalty parameter throughout the simulation, we were able to generate one case that showed plume lift-off. The results of this simulation are qualitatively comparable with the data given in Figures 7 and 8 and with the experimental data. Quantitatively, this penalty simulation experienced unrealistically large fluctuations in temperature. The expense of this trial-and-error method and the mediocre results convinced us not to pursue this technique on additional problems. Figure 4 (bottom) illustrates this performance for a plume simulation with $T_{amb} = 0{\cdot}1$ °C using $\varepsilon = 10^{-12}$.

We conclude from the above results that the neither the mixed nor the penalty method as used in the original NACHOS-II code is able to model the creeping thermal plume owing to the

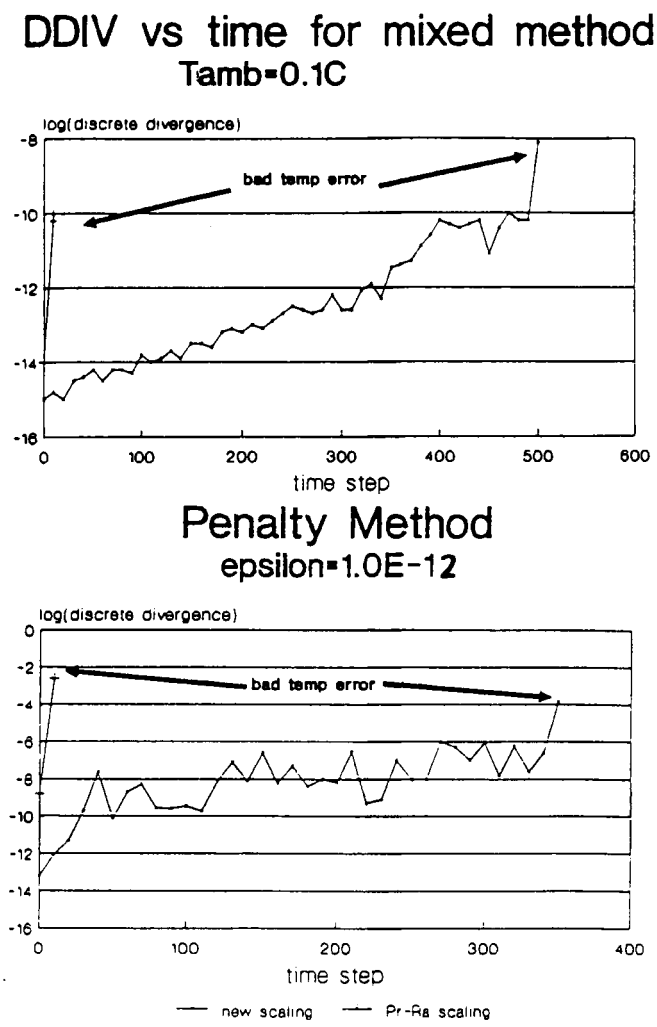

Figure 4. Discrete divergence DDIV for $T_{amb} = 0{\cdot}1$ °C as a function of the number of time steps (each of 11·3 s duration) for the mixed method (top) and the penalty method ($\varepsilon = 10^{-12}$) (bottom) and using the QUAD8, disc. p-element. In each plot the short vertical line which ends after about 10 time steps corresponds to the classical Ra–Pr-scaling of the governing equations and the other curve to the new scaling (Section 6)

inadequacy of both methods to satisfy sufficiently the div = 0 condition. In the following sections we report on some FE modifications and new approaches we have taken to attempt to achieve this goal.

6. NUMERICAL SIMULATIONS: TOWARDS THE GOAL TO ENFORCE THE DIVERGENCE-FREE CONSTRAINT

Improving the condition of the FE equations: effects of scaling

The positive numerical implications for DDIV of the new Pr-non-dimensionalization discussed earlier become clearer when viewed from the linear algebraic point of view, where it has the effect

of equilibrating the different magnitudes of the buoyancy B and the pressure matrices Q and B and the two viscous matrices K and L in equation (13) respectively. Assuming a consistent matrix norm $\|\cdot\|$ (which can be any Frobenius norm,[38] particularly l_1 or l_2), one can write $\|K\| = \|\lambda_1 B\|$, $\|Q\| = \|\lambda_2 B\|$ and $\|L\| = \|\lambda_3 B\|$, with $\lambda_1, \lambda_2, \lambda_3 \ll 1$ in equation (13). Then postmultiplying the global matrix in the system

$$\begin{pmatrix} \mathbf{K} & -\mathbf{Q} & \mathbf{B} \\ -\mathbf{Q}^{\mathrm{T}} & 0 & 0 \\ \mathbf{0} & 0 & \mathbf{L} \end{pmatrix} \begin{pmatrix} \mathbf{u} \\ \mathbf{p} \\ \mathbf{T} \end{pmatrix} = \begin{pmatrix} \mathbf{F} \\ \mathbf{0} \\ \mathbf{G} \end{pmatrix} \tag{23}$$

to be solved at each time step (assuming the convective terms $C(u)$ and $D(u)$ to be included in K and L respectively) by the diagonal matrix $\mathrm{diag}(1/\lambda_1, 1/\lambda_2, 1/\lambda_3)$ results in a rescaled system of equations of the form

$$\begin{pmatrix} \sim\mathbf{B} & -\sim\mathbf{B} & \sim\mathbf{B} \\ -\sim\mathbf{B}^{\mathrm{T}} & 0 & 0 \\ \mathbf{0} & 0 & \sim\mathbf{B} \end{pmatrix} \begin{pmatrix} \mathbf{u}^* \\ \mathbf{p}^* \\ \mathbf{T}^* \end{pmatrix} = \begin{pmatrix} \mathbf{F} \\ \mathbf{0} \\ \mathbf{G} \end{pmatrix}, \tag{24}$$

where $u^* = \lambda_1 u$, $p^* = \lambda_2 p$ and $T^* = \lambda_3 T$ are new, rescaled variables.

The Pr-scaling approach resulted in a marked improvement in the performance of the FEM code over that with the earlier Pr–Ra-scaling by forcing the terms in the matrices representing pressure, buoyancy and viscosity to be of about the same size and thus ameliorating the condition of the matrix. For example, whereas in the Pr–Ra-scaling with $Ra = 6{\cdot}5 \times 10^6$, values of $(\sim 10^{-2}, \sim 10^2)$ were found for a typical element (K, B) in equation (23), i.e. a difference of order $O(10^4)$ in magnitude, for the new scaling the corresponding values are $(\sim 10^2, \sim 10^2)$. Table II illustrates the ensuing positive effects on the discrete divergence, which is also reduced by several orders of magnitude. Nevertheless, in spite of these lower values for DDIV, Figure 4 reveals a similar disastrous behaviour of DDIV with simulation time and eventually numerical breakdown. Although this occurs at a much later time, demonstrating the advantage of the new scaling technique, the latter is still unable to successfully model a realistic thermal plume. For comparison, Table II includes a column representing the results of using the Pr–$Gr^{1/2}$-scaling (equations (6b) and (7b)) commonly used in engineering fluid mechanics. These results indicate that while this scaling would be acceptable for our problem, a slight improvement is often shown with the new scaling. Additionally, since we anticipate using this approach in Ra–Pr-ranges where the Pr–$Gr^{1/2}$-scaling may not be as favourable, we prefer to use the new scaling which is consistent with the physical processes involved (note that for large Gr the buoyancy term is much larger than the viscous term in equation (6b)).

Use of an iterated penalty method

As the next step in our goal to enforce the div = 0 condition, we have implemented an iterated penalty method which has been proposed for the FE solution of Stokes flow.[21,39] The iterated penalty approach is based on the dual role of the pressure (see Section 3) and attempts to better satisfy the incompressibility condition by an iterative, improved computation of the pressure. The algorithm used can be written as follows.[21]

1. Given $\mathbf{p}^{n-1}$, solve for $\mathbf{u}^n$ and $\mathbf{T}^n$ as

$$\begin{pmatrix} \mathbf{M} & 0 \\ 0 & \mathbf{N} \end{pmatrix} \begin{pmatrix} \partial\mathbf{u}/\partial t \\ \partial\mathbf{T}/\partial t \end{pmatrix} \begin{pmatrix} \mathbf{C(u)} + \mathbf{K(u, T)} & \mathbf{B(T)} \\ \mathbf{0} & \mathbf{D(u)} + \mathbf{L(T)} \end{pmatrix} \begin{pmatrix} \mathbf{u} \\ \mathbf{T} \end{pmatrix} = \begin{pmatrix} \mathbf{F(T)} + \mathbf{Q}\mathbf{p}^{n-1} \\ \mathbf{G(T, u)} \end{pmatrix}. \tag{25}$$

2. Update

$$\mathbf{p}^n = \mathbf{p}^{n-1} + (1/\varepsilon)\mathbf{M}_p^{-1}\mathbf{Q}^T\mathbf{u}^n. \tag{26}$$

3. Repeat steps 1 and 2 until the discrete divergence is small enough ($O(\varepsilon)$). Note that the traditional penalty method is imbedded in this method when $p^0 = 0$ and steps 2 and 3 are performed only once.

Results of numerical experiments with this method were generally poorer than those found with a full augmented Lagrangian formulation, to be described in the following section. In fact, viewed from the standpoint of constrained optimization,[29,39] the incompressibility is not enforced enough. This was also corroborated by the results of the numerical simulations, which often showed divergence of the iteration procedure and a large increase in DDIV as time progressed.

Use of an augmented Lagrangian method: the Uzawa algorithm

The technique of the augmented Lagrangian has been proposed, particularly by the French FE school,[24,26,28–30,39] as a powerful method for enforcing incompressibility in steady state Stokes flow. Fortin and Fortin[28] have extended it to the full, non-linear, steady state Navier–Stokes equations.

The augmented Lagrangian L_{aug} for the Stokes problem is defined in discrete matrix formulation as

$$L_{\text{aug}} = L + \beta|\mathbf{Q}^T\mathbf{u}|^2, \tag{27}$$

were L is the earlier defined regular Lagrangian (19) for the mixed (integrated) method. For the present non-linear NS problem the term $\frac{1}{2}\mathbf{K}\mathbf{u}^2$ in equation (19) is to be replaced by the Jacobian obtained from a quasi-linearization of the NS equation by means of a Newton method for example. Equation (27) illustrates that the div = 0 condition is enforced by penalizing the regular Lagrangian with the discrete incompressibility $\mathbf{Q}^T\mathbf{u}$, with β as the penalty or Lagrangian parameter.

For the minimization of L_{aug} in (27), the Uzawa algorithm,[26,28,29,39] which is a special form of conjugate gradient technique,[24] has been implemented. In the present case of the Boussinesq problem the iteration cycle for the Uzawa algorithm is written as

$$\begin{pmatrix} \mathbf{M} & 0 \\ 0 & \mathbf{N} \end{pmatrix}\begin{pmatrix} \partial\mathbf{u}/\partial t \\ \partial\mathbf{T}/\partial t \end{pmatrix}\begin{pmatrix} \mathbf{C}(\mathbf{u}) + \mathbf{K}(\mathbf{u},\mathbf{T}) + \beta\mathbf{Q}\mathbf{M}_p^{-1}\mathbf{Q}^T & \mathbf{B}(\mathbf{T}) \\ \mathbf{0} & \mathbf{D}(\mathbf{u}) + \mathbf{L}(\mathbf{T}) \end{pmatrix}\begin{pmatrix} \mathbf{u} \\ \mathbf{T} \end{pmatrix} = \begin{pmatrix} \mathbf{F}(\mathbf{T}) + \mathbf{Q}\mathbf{p}^{n-1} \\ \mathbf{G}(\mathbf{T},\mathbf{u}) \end{pmatrix}, \tag{28}$$

$$\mathbf{p}^n = \mathbf{p}^{n-1} + \gamma\mathbf{M}_p^{-1}\mathbf{Q}^T\mathbf{u}^n, \tag{29}$$

where β and γ are two freely (!) chosen Lagrangian parameters. There has been some discussion on the proper choice of β and γ, but the final jury is still out. As proven by Fortin and Glowinski[29] and Glowinski,[39] for sufficiently large β the convergence rate of the cycle (28), (29) is of order $O(1/\beta)$ and the optimal γ—which has to be determined from the eigenvalue spectrum of $\mathbf{K}^{-1}\mathbf{Q}^T\mathbf{Q}$—is $\beta \sim \gamma$. This has been assumed in the following simulations and without loss of generality we set $\beta = \gamma = 1/\varepsilon$, with ε the penalty parameter employed earlier.

This Uzawa method, which is straightforward to implement in most FE programmes, seemed very promising, particularly in the light of the excellent results obtained by Pelletier *et al.*[26] for the Stokes problem. They stated that for small ε, convergence of the discrete divergence DDIV to $O(\varepsilon)$ occurred with only one or two iterations. Rapid convergence is necessary for this method, since the global system (28) must be solved for each penalty iteration. Although some computa-

tional gain could be achieved in the present study by storing the factorized stiffness matrix in equation (28), the cost advantages of the penalty method over the ordinary mixed method are lost if more than two or three iterations are used.

Initial testing of the Uzawa algorithm showed very good results for short periods of time. Similarly to the behaviour of the regular penalty method, the value of ε greatly affected the performance of the algorithm. For the $T_{amb} = 25\,^{\circ}C$ benchmark plume problem on a 15×20 grid with $\Delta t = 0{\cdot}0003$, $\varepsilon = 10 \times 10^{-13}$ required 10 iterations, $\varepsilon = 3 \times 10^{-13}$ between five and seven iterations and $\varepsilon = 1 \times 10^{-13}$ only one iteration per time step to reduce DDIV to $O(\varepsilon)$. This sensitivity to ε is also reflected in the rate of convergence. Whereas after ~ 100 time steps $\varepsilon = 1 \times 10^{-13}$ decreased DDIV by roughly one order of magnitude per iteration, the convergence rates for $\varepsilon = 3 \times 10^{-13}$ and 10×10^{-13} are only $\sim 18\%$ and $\sim 10\%$ per iteration respectively. These observations appear to be consistent with those of Pelletier *et al.*[26] and Fortin and Glowinski.[29]

Extensive testing of the Uzawa algorithm for the plume problem, however, consistently demonstrated that the performance deteriorated as time progressed. Simulations that started with only one or two iterations per time step would often require four or five iterations after 100–200 time steps. A typical example was a simulation of the $T_{amb} = 25\,^{\circ}C$ experiment on a 25×30 grid with $\Delta t = 0{\cdot}01$. Whereas the first 70 time steps usually required only one Uzawa iteration per time step, the subsequent 50 time steps used already five or six iterations. This resulted in an overall CPU time for the Uzawa algorithm of 48 min as compared with only 16 min for the ordinary mixed method.

Figure 5 (top) illustrates the rate-of-convergence changes as the time integration progresses for the (more extreme) $T_{amb} = 0{\cdot}1\,^{\circ}C$ case and employing $\varepsilon = 1 \times 10^{-14}$. Since the convergence was highly dependent on the choice of ε, a single acceptable value for ε was never determined for an entire simulation. These results coincide with comments made by Fortin and Glowinski[29] for similar non-linear problems regarding the sensitivity of the Uzawa algorithm to the choice of ε. We found that without an adequate choice of ε the convergence was too slow to be economical when compared with the mixed method. These poor results led to abandonment of the Uzawa technique as described here. However, one possible option to be investigated in future studies to remedy the present negative situation will be the use of an adaptive ε as time progresses.

Use of a multistep Newton method

Although both the new scaling option and the Uzawa algorithm allowed us to further approach our goal of enforcing the div = 0 condition, they are incapable of successfully simulating a thermal plume under the extreme conditions observed in Figure 1. The reasons for this inadequacy may be manifold, but it is likely that many of the theoretical and numerical observations which have been made primarily for isothermal Stokes flow,[26–31] may not be valid for the present nonlinear Boussinesq plume problem.

As a final resort we investigate how far the non-linearity of the coupled flow/heat transport problem affects the performance of the present FEM. NACHOS-II uses Newton's method to solve the non-linear matrix system (13). Newton's method is quadratically convergent provided that the initial guess is close enough to the solution. Since NACHOS-II uses a predictor/corrector-type time integration, the predicted solution value will generally be close to the correct solution for each time step. This assumption provides the basis for NACHOS-II to use a one-step Newton method for the solution of the non-linear system. This approach appears to be also justified from the results of the numerical experiments of Gresho *et al.*,[40] though for isothermal flow. As discussed in Section 3, the non-linearity of the plume problem is accentuated in the

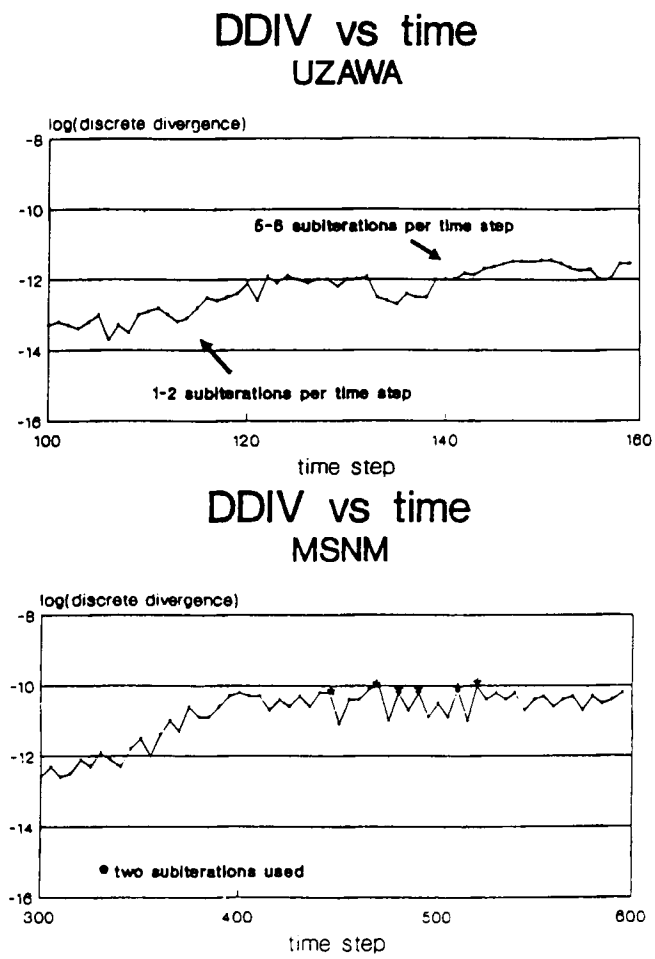

Figure 5. Discrete divergence DDIV for $T_{amb} = 0{\cdot}1$ °C as a function of the number of time steps (each of 11·3 s duration) within a certain window of the simulation: top, augmented Lagrangian (Uzawa algorithm), bottom, new multistep Newton method (MSNM) in the mixed FEM

present FE formulation by the specific, implicit coupling of the temperature in the energy equation to both pressure and velocity in the momentum equation over the presence of the non-linear buoyancy submatrix $B(T)$ in equations (13) and (14).

The modification made to NACHOS-II is a simple extension of the base logic. After the first Newton iteration the discrete divergence DDIV is used as a test of convergence. If DDIV is too large, an additional Newton iteration is completed. The process is repeated until DDIV is small enough (of the order of machine ε for the mixed method, with adjustments made for round-off error and higher velocities as the simulation progresses).

This multistep Newton method in conjunction with the new scaling gave acceptable results as reported in the next section. Since most time steps normally required only one Newton iteration, the extra cost was insignificant. Because of the quadratic rate of convergence of the Newton method, an additional Newton subiteration during a time step reduced the DDIV by

about one or two orders of magnitude, so that usually only two or three iterations are needed to decrease DDIV sufficiently. This is illustrated in Figure 5 (bottom) for the $T_{amb} = 0{\cdot}1$ °C case using the mixed FEM.

7. NUMERICAL SIMULATION OF PLUME EXPERIMENTS

The goal of the numerical simulations was to produce transient plume initiation and growth in an economical fashion that reflected the basic physics of the problem. Comparison of the simulation with experimental results would serve as valuable validation of the model. The arguments and computational data presented in the previous sections suggest that the best approach available for solving the thermal plume problem is to use the discontinuous pressure element in a mixed FEM employing the new scaling (non-dimensionalization) and the new multistep Newton method. We employed both QUAD8 and QUAD9 elements in our mesh refinement studies. On coarser meshes and the mesh chosen for the simulation we found the QUAD8 element to be superior in terms of time step flexibility and total run time for the grids used in the simulation. For example, QUAD9 required a time step one-tenth the size of QUAD8 for the run to be successful on the same grid, resulting in 7·5 h of CPU time for the QUAD9 element versus only 45 min of CPU time for QUAD8. This small time step, in addition to having more equations to solve owing to the additional node, made QUAD9 more than 10 times as expensive to run for the cases we considered. For the fine-mesh validations the QUAD9 element was more stable owing to its satisfaction of the LBB condition. The results of the following simulations show that through the combination of these options the FEM is able to accurately predict the growth and rise of some of the observed laboratory plumes of Coulliette.[7]

Ambient temperature of 25 °C

A mesh with 15 grid points in the radial and 50 grid points in the vertical direction was used. The node spacing in the radial direction was refined towards the axis of the plume above the heater. For all cases the maximum element size and time step were determined by the fundamental length and time scales used for the problem. On the basis of the theoretical accuracy of the FEM, these choices also ensured that the numerical resolution was greater than the error in the experimental measurements. The heater was represented by specifying a constant heat flux along the bottom of the first four elements. First-order Euler time integration was used early in the simulation to damp out temporal oscillations in the solution during the rapid heater initiation. After this start-up phase the more precise second-order time integration was employed (see Section 2). Using snapshots of the temperature contours for the delineation of the plume extension (similar to those shown in Figure 8 for the $T_{amb} = 0{\cdot}1$ °C plume case), the height versus time, $h(t)$, was visually determined for the top of the ball. The results obtained by measuring the location of the $T = 25$ °C contour are shown in Figure 6 (bottom) and are to be compared with those obtained from the experimental data (Figure 6, top). Note that since the numerical heater start-up was somewhat slower than the experimental one, the numerically obtained height values are somewhat less than the experimental ones during this initial stage of the simulation. At later times both plots display a relatively constant speed throughout most of the rise. For the experimental data this average speed is 0·055 cm s^{-1}, whereas the numerical simulation delivers 0·056 cm s^{-1}. Thise results agree within the error tolerance of the experimental data and thus demonstrate the power of the proposed FE technique.

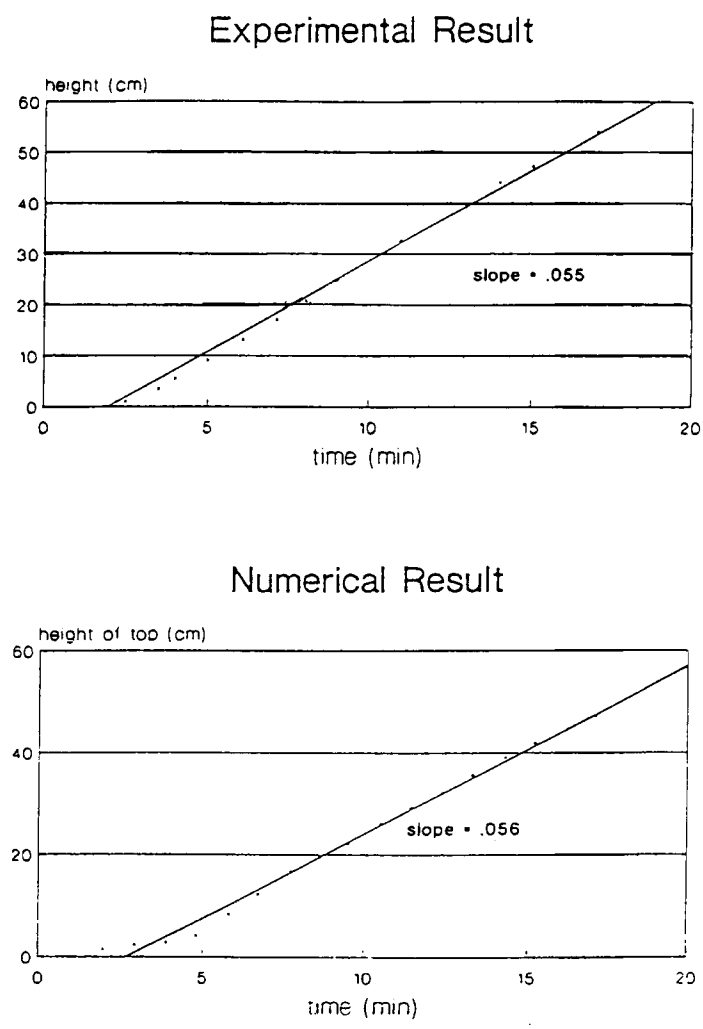

Figure 6. Height of the plume head as a function of time for the $T_{amb} = 25$ °C plume case: top, experimental results; bottom, numerical results

Ambient temperature of 0·1 °C

A 15 × 50 mesh similar to the previous $T_{amb} = 25$ °C case was also used here. However, a time-dependent heat flux boundary condition was used along the bottom of the first three elements to simulate a realistic heater start-up. The heat flux was increased gradually over a time period of 1·3 hours to the full power used in the experiment. This gradual increase, along with the damping from the Euler time integration, smoothed large temporal oscillations in the early steps of the simulation.

This slow heating (which is less than the experimental one but was necessary to dampen temporal oscillations during the onset of the plume) also shifted the plots of height versus time (measured from the $T = 15{\cdot}4$ °C contour) further apart (compared with the $T_{amb} = 25$ °C case) (Figure 7). However, once full heater power is achieved in the numerical simulation, the model fits the experimental behaviour very well. The average speed of the plume confirms this

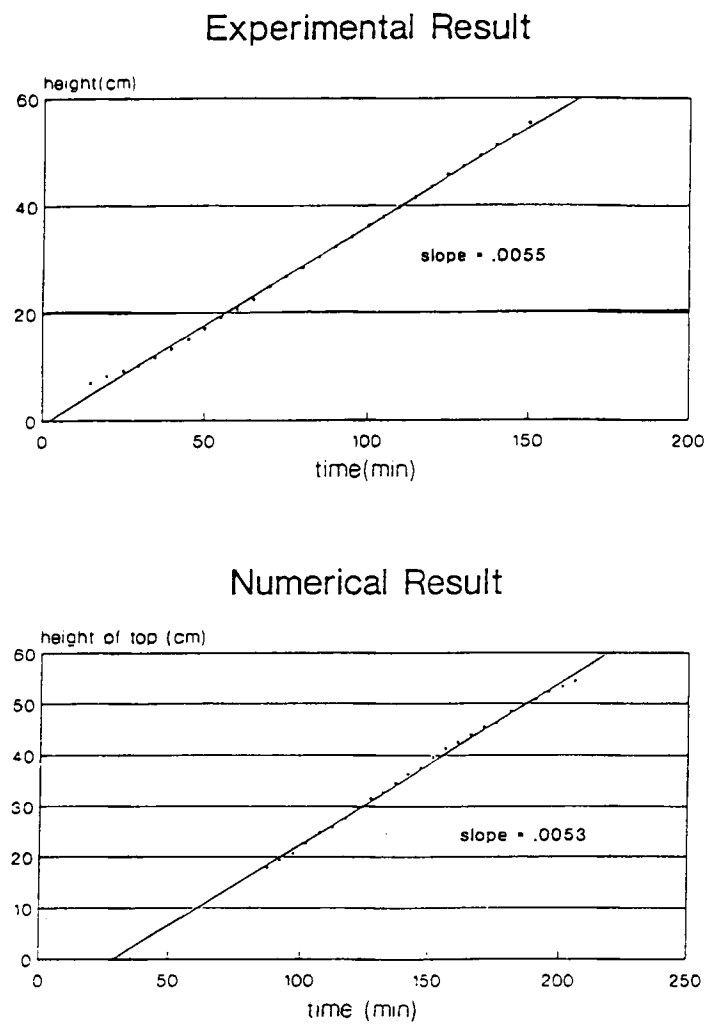

Figure 7. Height of the plume head as a function of time for the $T_{amb} = 0{\cdot}1$ °C plume case: top, experimental results; bottom, numerical results

observation since it agrees to within experimental accuracy—the experimentally and numerically determined speeds are 0·0055 and 0·0053 cm s^{-1} respectively. Figure 8 shows snapshots of the simulated plume for four different time steps. In addition to the linear rise, one also observes an increase in the radius of the ball, which, however, as shown by Coulliette,[7] follows a more complicated power law. Efforts are under way at present to use this information in an asymptotic scaling analysis of the thermal plume.

Ambient temperature of −26·1 °C

No successful runs were completed for this extreme temperature contrast between ambient medium and plume interior which produces a viscosity contrast of order $O(10^7)$. The resulting large differences in the magnitudes of the elements in the global stiffness matrix corresponding to viscous forces (matrix K in equation (13)) created too much ill-conditioning and subsequently

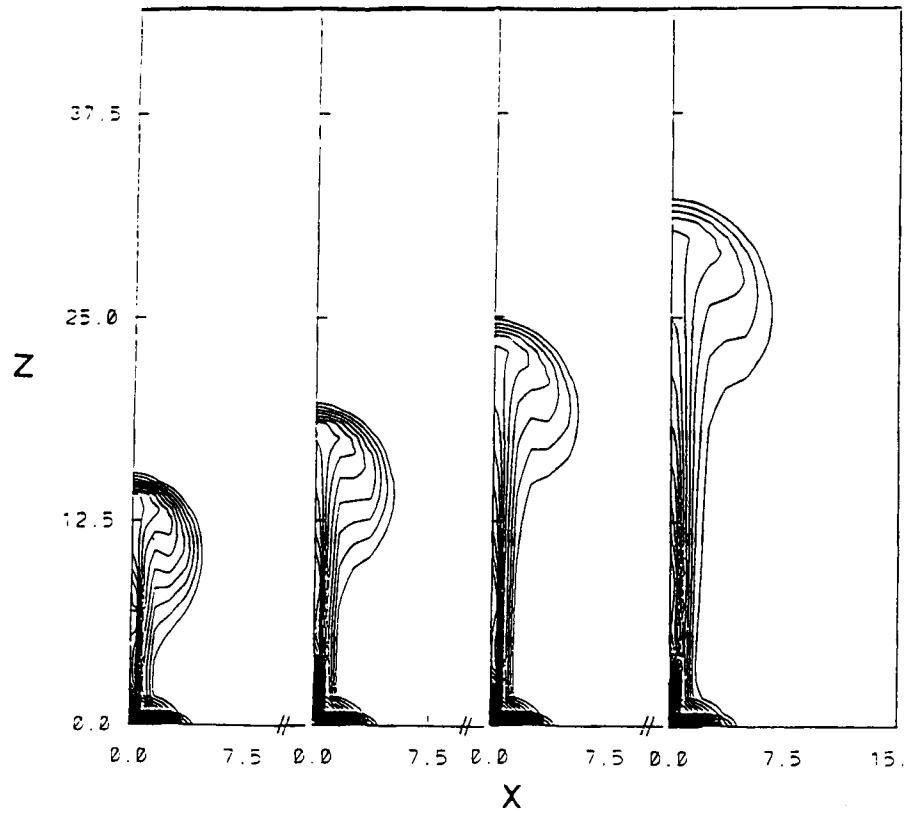

Figure 8. Snapshots of the plume temperature contours for the $T_{amb} = 0{\cdot}1$ °C plume case for four times, 1·5, 2·0, 2·5 and 3·1 h (from left to right). Axis lengths are non-dimensional (using the new scaling of Section 6) and are to be multiplied by a factor of 1·58 to get real dimensions. Only about one-third of the total width of the model is shown

caused failure of the solution process. Note that the earlier proposed new scaling does not balance such differences on an element level within the viscosity submatrix. Such an algebraic scaling of elements has been suggested by Pelletier *et al.*[26] for the solution of Stokes flow with large viscosity variations and will be investigated in the future.

8. CONCLUSIONS

Despite access to several standard element and solution options, the general-purpose Galerkin finite element package NACHOS-II proves inadequate to simulate experimentally observed thermal plumes in a medium with highly temperature-dependent viscosity. Extending the work of earlier steady state, isothermal studies in Cartesian geometry to transient, variable temperature, axisymmetric cylindrical geometry, we find that the computed estimate of divergence represents an inexpensive and valuable diagnostic tool for the qualitative and quantitative evaluation of the numerical solution process. Our investigation of several element and solution options reveals that many of the theoretically predicted characteristics of certain types of finite elements and scalings may not necessarily translate into a corresponding numerical behaviour. We conclude that the combination of proper scaling (based on the physics of the problem) and

a multistep Newton method is the most effective, but yet not universally satisfactory, in modelling this difficult problem.

Our investigations also suggest possible directions for future research. The Uzawa algorithm showed promise in enforcing incompressibility at low cost. A modified form of the Uzawa algorithm using a variable penalty parameter could be a fruitful approach. Since the coupling of the energy equation (3) and the momentum equation (1) might accentuate the overall non-linearity of the plume problem, solving the momentum and energy equations consecutively may improve the solution characteristics, but most likely at the expense of other numerical improprieties. Finally, scaling the equations at the element level in a fashion similar to what we have done at the global level should reduce the ill-conditioning of the global stiffness matrix due to large viscosity contrasts and allow even larger viscosity contrasts to be modelled.

ACKNOWLEDGEMENTS

We are particularly grateful to Dr. Dave Loper for suggesting the project and for his numerous valuable hits and comments on improving the paper. Thanks are also due to Dr. Michael Navon for advice concerning the finite element analysis. We also thank two anonymous reviewers whose comments helped us to significantly improve the paper. The computations were sponsored partly by the U.S. Department of Energy through Contract No. DE-FC05-85ER250000 to SCRI and partly by Florida State University through the allocation of supercomputer resources on the Cray-YMP.

REFERENCES

1. B. Gebhart, Y. Jaluria, R. L. Mahajan and B. Sammakia, *Buoyancy-induced Flows and Transport*, Hemisphere, New York, 1988.
2. D. L. Loper, 'Mantle plumes', *Tectonophysics*, **187**, 373–385 (1991).
3. D. L. Turcotte and G. Schubert, *Geodynamics, Application of Continuum Physics to Geological Problems*, Wiley, New York, 1982.
4. J. A. Whitehead, 'Buoyancy-driven instabilities of low viscosity zones as models of magma rich zones', *J. Geophys. Res.*, **91**, 9303–9314 (1986).
5. G. K. Batchelor, *An Introduction to Fluid Dynamics*, Cambridge University Press, Cambridge, 1967.
6. J. Happel and H. Brenner, *Low Reynolds Number Hydrodynamics*, Martinus Nijhoff, The Hague, 1983.
7. D. L. Coulliette, 'Initiation and development of creeping thermal plumes', *Ph.D. Thesis*, Department of Mathematics, Florida State University, Tallahassee, FL, 1992.
8. S. Morris, 'The effects of a strongly temperature dependent viscosity on slow flow past a hot sphere', *J. Fluid Mech.*, **124**, 1–26 (1982).
9. N. M. Ribe, 'Diapirism in the Earth's mantle: experiments on the motion of a hot sphere in a fluid with temperature dependent viscosity', *J. Volcanol.*, **16**, 221–245, (1983).
10. P. Olson, G. Schubert and C. Anderson, 'Plume formation in the D'-layer and the roughness of the core–mantle boundary', *Nature*, **327**, 409–413 (1987).
11. R. W. Griffiths, 'Dynamics of mantle thermals with constant buoyancy or anomalous interval heating', *Earth Planet. Sci. Lett.*, **78**, 435–446 (1986).
12. R. W. Griffiths and I. H. Campbell, 'Stirring and structure in mantle-starting plumes', *Earth Planet. Sci. Lett.*, **99**, 66–78 (1990).
13. J. A. Whitehead and D. S. Luther, 'Dynamics of laboratory diapir and plume models', *J. Geophys. Res.*, **80**, 705–717 (1975).
14. P. Olson and H. Singer, 'Creeping plumes', *J. Fluid Mech.*, **158**, 511–531 (1985).
15. E. M. Parmentier, D. L. Turcotte and K. E. Torrance, 'Numerical experiments on the structure of mantle plumes', *J. Geophys. Res.*, **80**, 4417–4424 (1975).
16. S. F. Daly and A. Raefsky, 'On the penetration of a hot diapir through a strongly temperature-dependent viscosity medium,', *Geophys. J. R. Astronam. Soc.*, **83**, 657–681 (1985).
17. W. Zhao and D. A. Yuen, 'The effects of adiabatic and viscous heating on plumes', *Geophys. Res. Lett.*, **14**, 1223–1226 (1987).
18. D. K. Gartling, 'NACHOS-II—a finite element computer program for incompressible flow problems: Part I—Theoretical background; Part II—User's manual', *SAND86-1817*, Sandia Laboratories, Albuquerque, NM, 1986.

19. D. K. Gartling, 'NACHOS—a finite element computer program for incompressible flow problems: Part I—Theoretical background; Part II—User's manual', *SAND77-1334*, Sandia Laboratories, Albuquerque, NM, 1977.
20. M. Koch and D. A. Yuen, 'Surface deformation and geoid anomalies over single- and double-layered convection systems', *Geophys. Res. Lett.*, **12**, 701–704 (1985).
21. M. D. Gunzburger, *Finite Element Methods for Viscous Incompressible Flows*, Academic, Boston, MA, 1989.
22. C. Cuvelier, A. Segal and A. van Steenhoven, *Finite Element Methods and Navier–Stokes Equations*, Reidel, Dordrecht, 1986.
23. T. J. R. Hughes, *The Finite Element Method*, Prentice-Hall, Englewood Cliffs, NJ, 1987.
24. V. Girault and P. A. Raviart, *Finite Element Methods for Navier Stokes Equations*, Springer, New York, 1986.
25. D. S. Malkus, 'Advanced topics in the theory of mixed and penalty methods: pressure modes and error estimates', in T. J. R. Hughes (ed.), *The Finite Element Method*, Prentice-Hall, Englewood Cliffs, NJ, 1987, pp. 276–309.
26. D. Pelletier, A. Fortin and R. Camarero, 'Are FEM solutions of incompressible flows really incompressible? (or how simple flows can cause headaches!)', *Int. j. numer. methods fluids*, **9**, 99–112 (1989).
27. R. Sani, P. M. Gresho, R. L. Lee and D. F. Griffiths, 'The cause and cure (?) of the spurious pressures generated by certain FEM solutions of the incompressible Navier–Stokes equations, Parts I and II', *Int. j. numer. methods fluids*, **1**, 17–43, 171–204 (1980).
28. M. Fortin and A. Fortin, 'A generalization of Uzawa's algorithm for the solution of the Navier–Stokes equations', *Commun. Appl. Numer. Methods*, **1**, 205–210 (1985).
29. M. Fortin and R. Glowinski, *Augmented Lagrangian Methods: Applications to the Numerical Solution of Boundary-value Problems*, North-Holland, Amsterdam, 1983.
30. M. Fortin and S. Boivin, 'Iterative stabilization of the bilinear velocity–constant pressure element', *Int. j. numer. methods fluids*, **10**, 125–140 (1990).
31. J. Atang and D. Silvester, 'Iterative methods for stabilized mixed velocity–pressure finite elements', *Int. j. numer. methods fluids*, **14**, 71–81 (1992).
32. C. D. Upson, P. M. Gresho and R. L. Lee, 'Finite element simulations of thermally induced convection in an enclosed cavity', *Lawrence Livermore Laboratory Rep. UCID-18602*, 1980.
33. S. Ostrach, 'Natural convective heat transfer in cavities and cells', *J. Heat Transfer*, **1**, 365–378 (1980).
34. T. Y. Chu and C. E. Hickox, 'Thermal convection with large viscosity variation in an enclosure with localized heating', *ASME J. Heat Transfer*, **112**, 388–395 (1990).
35. C. E. Hickox and T. Y. Chu, 'Developing natural convection in a fluid layer with localized heating and large viscosity variations', *ASME FED*, **107**, 75–81 (1991).
36. P. M. Gresho, R. L. Lee, S. T. Chan and J. M. Leone Jr., 'A new finite element for incompressible Boussinesq fluids', *Proc. Third Int. Conf. on Finite Elements*, Banff, June 1980, pp. 204–215.
37. F. Brezzi and J. Douglas, 'Stabilized mixed methods for the Stokes problem', *Numer. Math.*, **53**, 225–235 (1988).
38. G. H. Golub and C. F. Van Loan, *Matrix Computations*, Johns Hopkins University Press, Baltimore, MD, 1989.
39. R. Glowinski, *Numerical Methods for Nonlinear Variational Problems*, Springer, New York, 1984.
40. P. M. Gresho, R. L. Lee and R. Sani, 'On the time-dependent solution of the incompressible Navier–Stokes equations in two and three dimensions', in C. Taylor and K. Morgan (eds.), *Recent Advances in Numerical Methods in Fluids*, Vol. I, Pineridge, Swansea, 1980, pp. 27–81.